Article

Low-noise frequency synthesis and terahertz wireless communication driven by compact turnkey Kerr combs

Kunpeng Jia [1,6] ✉, Yuancheng Cai [2,3,6], Xinwei Yi[1,6], Chenye Qin[1,6], Zexing Zhao[1], Xiaohan Wang[1], Yunfeng Liu[4], Xiaofan Zhang[1], Shanshan Cheng[1], Xiaoshun Jiang [1], Chong Sheng [1], Yongming Huang [2,3] ✉, Jianjun Yu[2,5], Hui Liu [1], Biaobing Jin [1,2], Xiaohu You[2,3], Shi-ning Zhu[1], Wei Liang[4] ✉, Min Zhu [2,3] ✉ & Zhenda Xie [1] ✉

High frequency microwave, spanning up to terahertz frequency, is pivotal for next-generation communication, sensing and radar. However, it faces fundamental noise limitations when frequency is pushed towards such boundary of conventional electronic technologies. Photonic microwave generation, particularly Kerr-comb-based microwave source, benefits from high frequency operation but still suffers from phase noise constraints. Here we overcome this drawback by developing a compact, electrically-driven Kerr comb system that achieves near quantum-limited phase noise for microwave synthesis up to 384 GHz. Leveraging high-Q fiber Fabry-Perot resonators and optimized noise modeling under limited pump power, we demonstrate ultra-low phase noise performances of −133 dBc/Hz (10.1 GHz) and −95 dBc/Hz (300 GHz) at 10 kHz offset, approaching quantum noise limits. This breakthrough enables 64QAM modulation in terahertz wireless communication and record 240 Gbps data rate without need for carrier phase estimation. Our device can serve as a key building block for the future information technology.

The new generation of wireless communication, remote sensing, and imaging applications calls for advanced high-frequency microwave technology, towards large channel bandwidth as required by the demand of the high data rate[1–7]. The other side of the coin for such a high data rate, as limited by the Shannon–Hartley theorem, relies on the low phase noise, to achieve a high signal-to-noise ratio (SNR) to take full advantage of the broad bandwidth[8–10]. However, the common electronic technology has its limit for the low-noise generation of high-frequency microwave, especially when the frequency scales up

towards terahertz ranges. Such a limit may be overcome via photonic microwave frequency generation, taking advantage of the high-coherence optical sources such as optical frequency combs (OFCs)[11–17]. Specifically, the recent progress in the comb generation using a monolithic Kerr resonator (Kerr comb)[18,19] can further pack the OFC precision towards a field-deployable frequency synthesizer, and its small cavity size is inherently suitable for the high-frequency microwave generation, extending up to the terahertz range. In such a small mode volume, the strong nonlinear optical interaction also

[1]National Laboratory of Solid State Microstructures, School of Electronic Science and Engineering, College of Engineering and Applied Sciences, School of Physics, Research Institute of Superconductor Electronics (RISE) & Key Laboratory of Optoelectronic Devices and Systems with Extreme Performances of MOE, Key Laboratory of Intelligent Optical Sensing and Manipulation, Ministry of Education, and Collaborative Innovation Center of Advanced Microstructures, Nanjing University, Nanjing, China. [2]Purple Mountain Laboratories, Nanjing, China. [3]National Mobile Communications Research Laboratory, Southeast University, Nanjing, China. [4]Key Laboratory of Semiconductor Display Materials and Chips, Suzhou Institute of Nano-tech and Nano-bionics, Chinese Academy of Sciences, Suzhou, China. [5]Fudan University, Shanghai, China. [6]These authors contributed equally: Kunpeng Jia, Yuancheng Cai, Xinwei Yi, Chenye Qin. ✉e-mail: jiakunpeng@nju.edu.cn; huangym@seu.edu.cn; wliang2019@sinano.ac.cn; minzhu@seu.edu.cn; xiezhenda@nju.edu.cn

reduces the pump power requirement and enables a compact package size.

However, the conventional Kerr combs based on microresonators suffer from higher noise in comparison to the mode-locked-laser-based OFCs, as the side effect of the limited mode volumes. On the one hand, the strong nonlinearity in small mode volume sets a relatively high quantum noise limit[20,21], and on the other hand, such quantum limit is not easily accessible because of the pump laser noise, thermorefractive noise, etc., as raised in the small mode volume. Thus, it is a fundamental question that whether a Kerr comb can be built with a lower pump power requirement for direct diode pump, and capable of high-frequency and low-noise microwave generation up to terahertz frequency.

Here we answer this question by the demonstration of the first low-noise frequency synthesis ranging from 10.1 to 384 GHz in a compact electric-driven turnkey Kerr comb package. Low quantum noise limit is engineered following our theoretical noise analysis with limited pump power and the state-of-the-art fabrication of a high-quality factor (Q) of 6.0×10^8 using a few-mode-fiber-based Fabry-Perot resonator (FFPR). This FFPR device enables low-noise Kerr comb generation in a compact and pump-diode-integrated setup within $85 \times 90 \times 25$ mm. Phase noises of -133 dBc/Hz and -95 dBc/Hz at 10 kHz, and -160 dBc/Hz and -133 dBc/Hz noise floors are measured at 10.1 GHz and 300 GHz repetition rates, respectively, for the single soliton and soliton crystal states, which scale consistently and are both close to the quantum noise limit. Turnkey operations are achieved without dynamic tuning, with a high access rate near unity. Low Allan deviation is measured for 4×10^{-10} at 1 s averaging time, showing good long-term stability in a fully free-running setup. With this low phase noise performance, high-speed terahertz wireless communication up to 240 Gbps is demonstrated, which is free of carrier phase estimation (CPE), thus simplifying the digital signal processing (DSP). Above results mark a major step for Kerr combs towards field-deployable low-noise microwave generation, for radar[22,23] and communication[24] applications.

Results

The phase noise of a normal Kerr comb is higher than the OFCs based on mode-locked lasers, due to its limited mode volume. However, it is also the small mode volume, i.e., the strong light confinement for high nonlinearity, that lowers the pump power requirement, so as to enable a fully integrated direct-diode-pumped setup. Thus, it is an interesting and fundamental problem to study the low-noise generation of a Kerr comb while keeping the benefit of low pump power. The noise performance of a Kerr comb is fundamentally limited by the quantum noise, which is further affected by the pump noise and thermorefractive noise on top of the quantum noise. We model all these noises for the development of our FFPR Kerr resonator.

The previous study shows low quantum noise limit can be achieved with low Q and large mode area[21], which inevitably increases the pump power. Here we rewrite the equation for the quantum noise, and find that high Q actually helps to reduce the quantum noise, with the pump power limited. The quantum-limited phase noise L_Φ can be written in Eq. (1)[21,25–27], assuming the mode-locked soliton state is generated at certain ratio κ for pump power P_{in} relative to parametric threshold power P_{th}, (see details in Supplementary Information)

$$L_\Phi = \frac{\sqrt{2}\pi^3 \hbar c}{\lambda}\sqrt{\frac{1}{\kappa(-D)}}\frac{1}{P_{th}}, f >> \gamma$$
$$L_\Phi = \frac{\sqrt{2}\pi^5 \hbar c^3}{\lambda^3}\sqrt{\frac{-D}{\kappa}}\left[\frac{1}{96\kappa}+\frac{\kappa}{24\pi^2}\right]\frac{1}{f^2}\frac{1}{P_{th}Q^2}, f << \gamma \tag{1}$$

where D, γ, c, $\hbar$, λ, and f are the dimensionless dispersion parameter, half width half maximum of the cavity resonance, speed of light in the vacuum, reduced Planck's constant, pump wavelength, and the offset frequency, respectively. While the quantum noise at high offset

frequency is only related to the pump power, the noise at low offset frequency is inversely proportional to Q^2 at certain pump power. Indeed, phase noise at such low offset frequency plays an important role in the microwave frequency generation, as γ still covers the frequency of kilohertz with a high Q of 10^9.

On the other hand, it is crucial to reduce the pump noise limit L_P and the thermorefractive noise limit L_T to be lower than L_Φ in wide offset frequency range, for achieving quantum-limited performance. With a large mode volume of the FFPR, our simulation shows that the thermorefractive noise can be lower than the quantum noise limit from low offset frequencies above 100 Hz, so that reducing the pump noise is the key to achieving quantum-limited performance. The lower limit of L_P at the Kerr comb repetition rate is the frequency division from the pump noise[14,28], by the number N of comb lines. In a self-injection locking setup, significant noise reduction can be achieved when the Kerr resonator has much higher Q than that of the laser diode Q_{LD}[29–31] as

$$\eta = 1 + \frac{Q}{Q_{LD}}\sqrt{\beta(1+\alpha_g^2)}, \tag{2}$$

so that

$$L_P \geq \frac{L_{LD}}{\eta N^2}, \tag{3}$$

where β and α_g are the feedback strength and linewidth-broadening factor, respectively, L_{LD} is the phase noise of original laser diode. Equation (3) shows that high Q is also the key to reduce the pump noise and so as the pump-induced comb noise.

We choose to use few-mode fiber (from Yangtze Optical Fiber and Cable Joint Stock Limited Company) for the FFPR fabrication. This fiber exhibits only two transverse modes at 1550 nm, which is the key to ensuring the fundamental mode parametric oscillation and avoiding the mode-crossing effect. The Kerr nonlinear index n_2 is 3×10^{-20} m²/W, which is lower than that of normal silicon nitride material (2.5×10^{-19} m²/W). Despite of the few-mode design, large fundamental mode field area of 112 µm² results in the low phase noise, and the remaining challenge is to fabricate high enough Q to lower the pump power, to enable a direct diode pump setup as shown in Fig. 1a. Here the pump power is limited to about 100 mW from commercially available single mode distributed feedback (DFB) laser diode. We develop fine mechanical polishing and high-quality dielectric coating technologies for high-Q FFPR fabrication. The fused-silica-based fiber is mounted in a ceramic ferrule with an outside diameter of 2.5 mm and a length of 10 mm, finely polished, and then coated with 17-layer pairs of Ta_2O_5 and SiO_2 using the ion-assisted deposition method. Such a Bragg mirror achieves a reflectivity of over 99.99% at around 1550 nm. The FFPR with length of 10 mm (Fig. 1b) features a free spectral range of 10.1 GHz. The Q of the FFPR is characterized by cavity ring-down measurement[32]. By fast sweeping the frequency of a tunable external cavity diode laser (CTL 1550, Toptica) over the FFPR resonance, the decay time is fitted to be 492 ns, corresponding to Q of 6.0×10^8 (Fig. 1c). The high Q is attributed to two aspects. Firstly, the fiber we used features ultra-low attenuation of below 0.2 dB/km, corresponding to a fiber-propagation-loss-limited Q on the order of 10^{11}. Secondly, we adopt fine polishing technology to achieve a low surface roughness down to 1.57 nm in root mean square value. Such smooth end faces ensure low diffraction loss on the high-reflectivity mirror coating. It is interesting to compare the quantum noise limit, pump noise limit, and thermorefractive noise limit for our FFPR, which is plotted in Fig. 1d. The pump noise limit is calculated from the noise of the unlocked free-running DFB laser as shown in Fig. 1e, and taking into account the self-injection locking linewidth narrowing and frequency division effects. We find that the crossing frequency is around 100 Hz, above which it

can be possible to achieve quantum noise without being limited by the pump noise as well as thermorefractive noise. Of note, the noise at such low offset frequencies can be further suppressed by active feedback control, whose bandwidth is normally on the order of kilohertz.

Our Kerr comb setup is schematically shown in Fig. 1f. With a pump laser diode integrated, the whole setup is compact and fully electric-driven. The pump light from a DFB laser diode is directed through the FFPR for Kerr comb generation, with part of the transmission feedback into the laser diode, for self-injection locking[33]. In the experiment, the whole setup is assembled in a metal box with size of 85 × 90 × 25 mm, as shown in the inset of Fig. 1f. In the box, the DFB laser diode with its chip-on-carrier is attached directly on the metal baseplate, and all the micro-optics components, including half-wave plates (HWPs), high-reflection mirrors, a silicon sheet, monitor photodetector chip, Faraday rotator (FR), and polarizing beam splitter

(PBS) are integrated on the same baseplate. Temperature control is applied to the baseplate using the thermal electric component underneath. The optical feedback phase can be fine-tuned by the resistive heating of the silicon sheet in the feedback loop. Figure 1g is the picture of the Kerr comb setup with its actual footprint of 27 × 57 mm. It is worth noting that the components and assembling techniques we use for packaging this Kerr comb are similar to those used in the optical communication industry, so that our Kerr comb setup can be mass-produced when necessary.

We first characterize the pump laser performance in the setup for Kerr comb generation. The frequency noise of the pump is measured in comparison to its non-locked free-running state, using the correlated delayed self-heterodyne method[34], as shown in Fig. 1e. This is a general method for narrow fundamental linewidth measurement based on short optical delay. The setup consists of 1 km fiber for time delay and a 40 MHz acoustic optical modulator for frequency shift (see
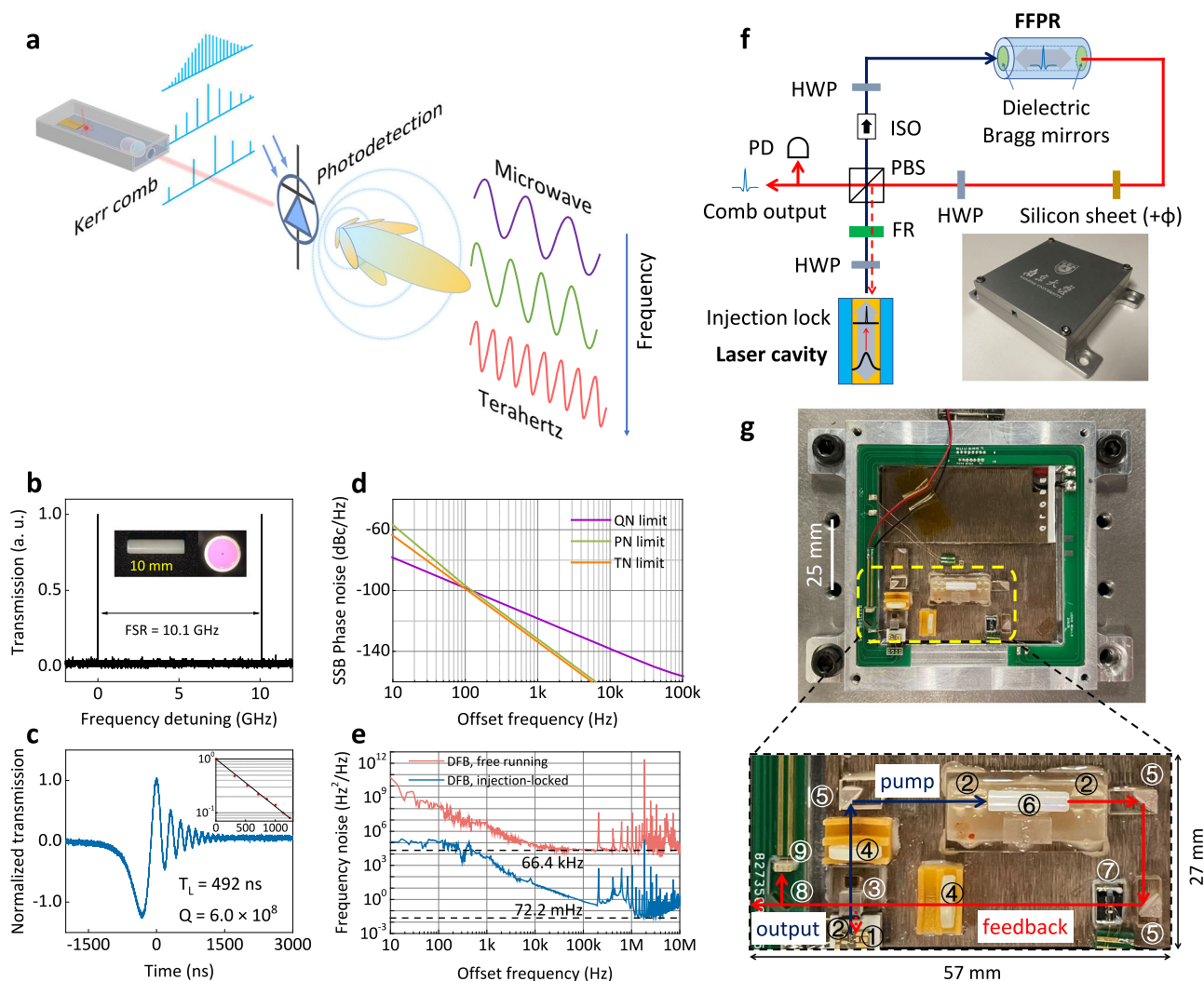

Fig. 1 | Compact Kerr comb package based on FFPR. a Frequency synthesizer driven by a compact Kerr comb source. **b** Transmission spectrum around 1550 nm of FFPR. Inset: picture of FFPR and microscope photo of the end face. **c** Ring-down trace of FFPR. Inset: fitted trace in logarithmic scale. **d** Quantum noise (QN) limit, pump noise (PN) limit, and thermorefractive noise (TN) limit of FFPR. The parameters used in the calculation are as follows: $Q_{LD} = 4 \times 10^3$, $\beta = 0.1$, and $\alpha_g = 2.5$[29-31]. $n_2 = 3 \times 10^{-20}$ m²/W, effective mode field area $A_{eff} = 112$ µm², group velocity dispersion (GVD) $\beta_2 = -27$ fs²/mm, $P_{in} = 100$ mW, $\lambda = 1545$ nm, $n = 1.45$. **e** Frequency noise spectral densities of the DFB laser with free-running state (red curve) and injection-locked to the FFPR (blue curve). 1 km of delay fiber is used. The dashed lines label

the fundamental linewidth levels, indicating a noise reduction factor of over 10⁵. **f** Schematic of our Kerr comb setup. Inset: picture of the package with a size of 85 × 90 × 25 mm. **g** Picture of the Kerr comb setup inside the package. ①, DFB laser diode (chip-on-carrier); ②, collimating lens; ③, a set of half-wave plates (HWP), Faraday rotator (FR), and polarizing beam splitter (PBS); ④, HWPs; ⑤, reflective mirrors; ⑥, FFPR; ⑦, silicon phase sheet; ⑧, beam splitter; ⑨, monitor photodetector. The solid blue, solid red, and dashed red curves represent for pump beam from the DFB laser diode, the comb beam from the FFPR, and the feedback beam to the DFB laser diode, respectively.
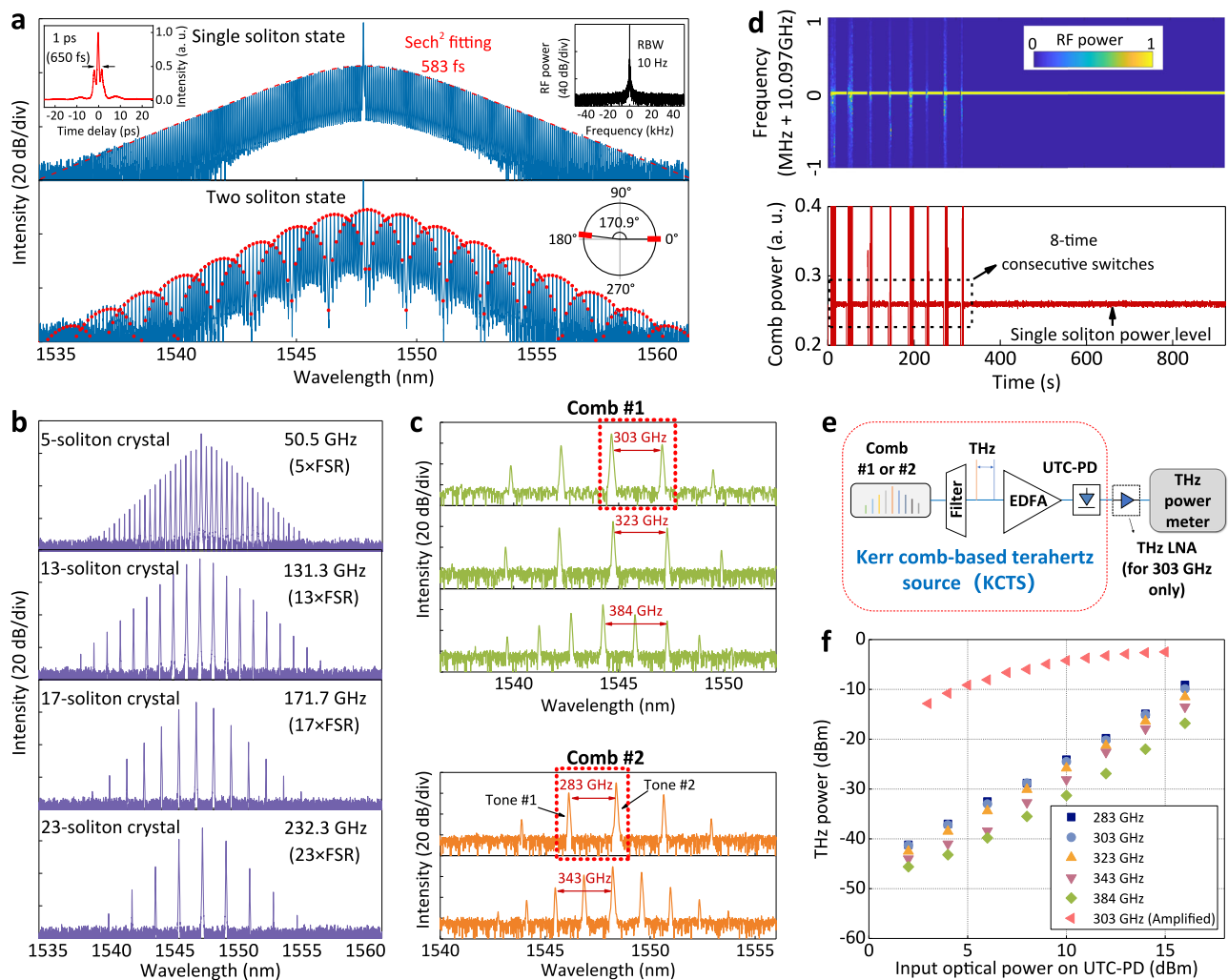
Fig. 2 | Soliton states generation for broadband frequency synthesis. a Upper panel: optical spectrum of a single soliton state. Left inset: autocorrelation trace of single soliton pulse. Right inset: RF beatnote of single soliton state centered at 10.1 GHz. RBW, resolution bandwidth. Lower panel: optical spectrum of a two-soliton state. Inset shows the relative phase position of the solitons in a round-trip inside the FFPR. **b** Optical spectra of soliton crystal states with different comb spacings. **c** Optical spectra of soliton crystal states in two Kerr comb packages. **d** 8-time consecutive switches test for turnkey operation. The top panel is a spectrogram of the soliton repetition rate signal measured during the switching process. The bottom panel shows the measured comb power as a function of time. **e** Setup of the Kerr comb-based terahertz source (KCTS). EDFA erbium-doped fiber amplifier, UTC-PD uni-traveling-carrier photodiode, LNA low-noise amplifier. **f** Measured terahertz power as a function of input optical power on UTC-PD.

details in Supplementary Information). Note that the spikes at 207 kHz and its harmonics are not the real frequency noise of the laser but simply a measurement artifact induced by the unbalanced interferometer used in this method. Ultra-narrow fundamental linewidth of 72.2 mHz is measured for the DFB laser injection-locked to the FFPR. Compared to the 66.4 kHz fundamental linewidth of a free-running DFB laser, a linewidth reduction factor near 10^6 is achieved. For the noise at 10 Hz offset frequency, the noise reduction is on the order of 50 dB, which agrees well with the theoretical calculation using Eq. (2) and the parameters presented in the caption of Fig. 1d. The purified pump spectra can be delivered to every comb line in following Kerr comb mode-locking, and found a good basis for the low-noise comb generation.

Different soliton states can be observed at different pump currents and feedback phases, including a single soliton state as well as perfect soliton crystal states. All of them have a smooth profile in the spectrum. Figure 2a shows the spectra of single soliton (upper panel) and two-soliton (lower panel) states with fundamental repetition rate of 10.1 GHz. The dashed red curve is a sech² spectral fitting for the

single soliton envelopes, and corresponds to a Fourier-transform pulse width of 583 fs. The measured temporal autocorrelation trace is plotted in the left inset of Fig. 2a upper panel, with 1 ps trace duration. An actual pulse width can be calculated to about 650 fs, which agrees well with the expectation from the optical spectrum. By sending the amplified single soliton comb with pump filtered into a fast photodetector, the beatnote signal is captured on an electrical spectrum analyzer (ESA) as shown in the right inset of Fig. 2a upper panel, revealing highly coherent mode-locked state generation. Perfect soliton crystal states can also be accessed, with comb spacings ranging from tens of GHz to hundreds of GHz (Fig. 2b). This means there are multiple equally spaced pulses in a round-trip, which effectively increases the repetition rate of the Kerr comb[35]. However, it is much more challenging for soliton crystal states with a high repetition rate to achieve high pulse energy as required for effective measurement using the autocorrelator. We show its simulated time-domain pulse trace in Supplementary Information. Different soliton states can be achieved by changing the pump laser frequency detuning relative to the resonance of the FFPR. The pump laser frequency can be directly tuned by
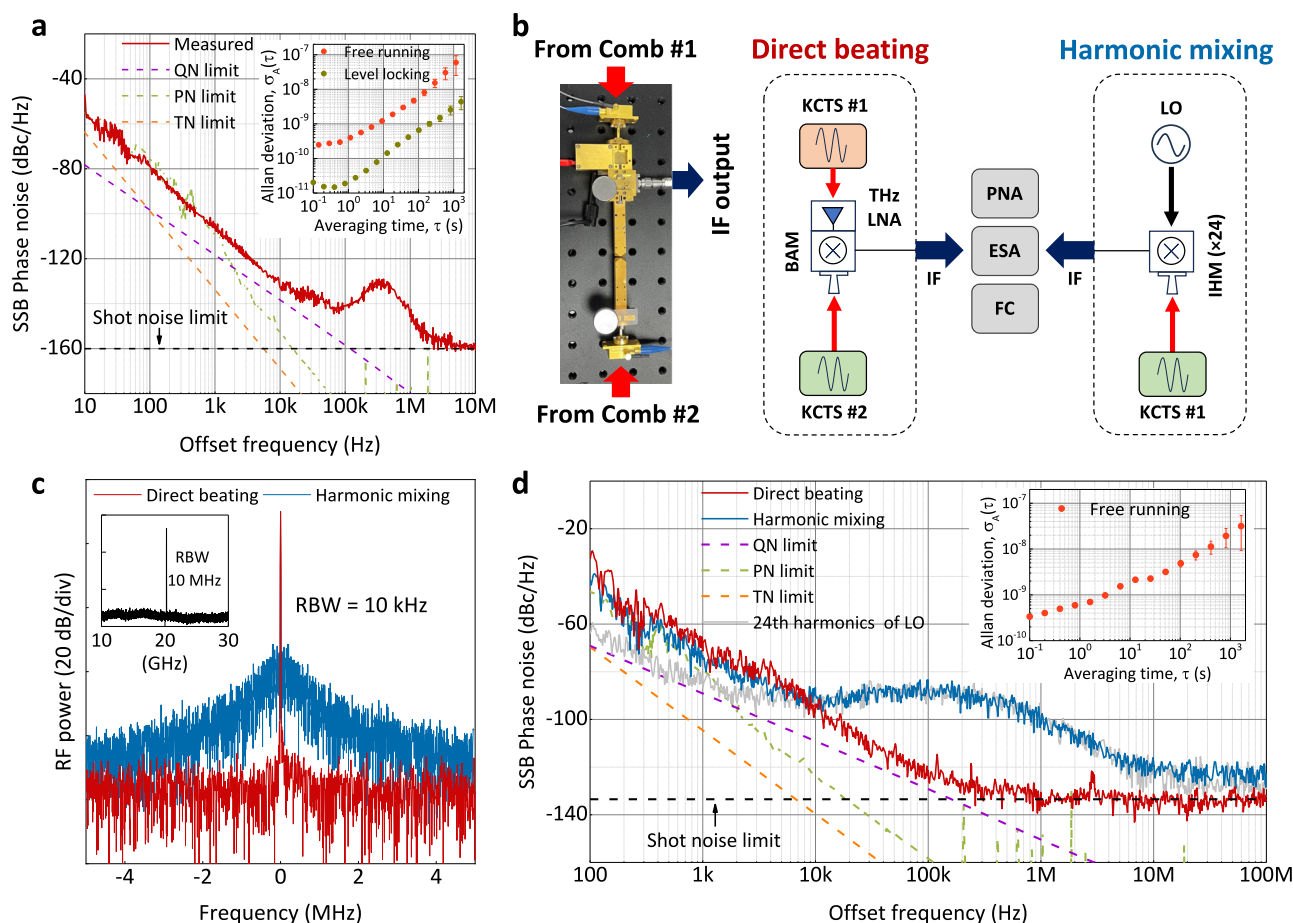
Fig. 3 | Noise characterization of the frequency synthesizer. a Single sideband (SSB) phase noise of 10.1 GHz repetition rate for single soliton state. The dashed purple and orange lines represent the calculated quantum noise (QN) and thermorefractive noise (TN) limits, respectively. The dashed green line represents the pump noise (PN) limit of the injection-locked pump laser, whose frequency noise is shown in Fig. 1e. The noise peaks that appear at 100–200 Hz offset frequency of the pump noise curve are likely to be caused by the vibration of the delay fiber in the heterodyne measurement system. Inset: Allan deviation results of single soliton repetition rate with free-running state (red) and level locking (yellow), which are measured using a frequency counter with a 10 MHz Rubidium clock signal as time base (0.1 s gate time). The error bar indicates the standard error of the mean.

b Setups of direct beating and harmonic mixing measurements. A terahertz LNA is used to increase the power of KCTS #1 to meet the requirement of the LO port in direct beating measurement. The generated IF signals are sent to microwave electronics for noise analysis. PNA phase noise analyzer, ESA electrical spectrum analyzer, FC frequency counter. **c** The spectra of down-converted microwave signals from direct beating (red) and harmonic mixing (blue). Inset: RF spectrum of the direct beating signal. **d** SSB phase noise of terahertz frequency measured with direct beating and harmonic mixing. Inset: Allan deviation of the terahertz frequency, which is measured using a frequency counter with a 10 MHz Rubidium clock signal as a time base (0.1 s gate time). The error bar indicates the standard error of the mean.

changing the current injected into laser diode. Figure 2c shows the spectra of soliton crystal states of two Kerr comb setups, marked as "Comb #1" and "Comb #2", respectively, and different terahertz repetition rates can be stably generated for each setup.

Our simulation shows that the soliton states generation can be achieved without dynamic tuning (see details in Supplementary Information), which agrees with the easy generation of the soliton states in the experiment. Even though it is sensitive to the feedback phase, the silicon sheet used for tuning the feedback phase via resistive heating features a high efficiency of $1\pi/V$ and high resolution of 0.001 V, which is sufficient to guarantee the excitation of the single soliton state. This effect is similar to the other case of Kerr comb generation using on-chip resonators[36,37]. Taking the single soliton state as an example, we test this turnkey effect with results shown in Fig. 2d. By keeping the temperature controller on for the baseplate and the silicon sheet, the single soliton state is built once the laser diode current is turned on and remains till the current is the turned off. RF beatnote frequency and comb power stay consistently between multiple switches, indicating excellent stability and reliability for the turnkey operation. Note that the soliton crystal states can also be

generated through such turnkey operation (see details in Supplementary Information), which is utilized for THz frequency synthesis in the following.

Then we characterize the stability and phase noise of this Kerr comb-based frequency synthesizer. We measure the phase noise of the single soliton state with repetition rate of 10.1 GHz using a phase noise analyzer (APPH40G, Anapico). The result is shown in Fig. 3a, in comparison with the quantum noise limit, pump noise limit, and thermorefractive noise limit. The measured phase noise is close to the quantum limit, especially for offset frequencies higher than 1 kHz. Note that the phase noise −160 dBc/Hz at high offset frequencies is limited by the shot noise of the photodetector. Further noise reduction can be expected with improvement of the fabrication technique for even higher Q. The long-term stability of the repetition rate is characterized by Allan deviation measurement, which is below 4×10^{-10} at 1 s and 5×10^{-9} at 100 s averaging time, respectively, as shown in the inset of Fig. 3a. The repetition rate can be tuned by the current tuning for the pump laser diode, for the range up to 1 kHz, which corresponds to 10^{-7} fraction of the 10.1 GHz carrier frequency. The frequency modulation efficiency is 1.3 kHz/mA. Such a tuning range is larger than the long-

term frequency drift over hours. We perform a simple test for stabilizing the comb repetition rate by level locking the comb power with active feedback control on pump current. The frequency instability can be reduced by an order of magnitude compared to that of the free-running case, as shown in the inset of Fig. 3a. Higher stability can be achieved by active feedback locking to a microwave frequency reference when necessary.

We use uni-traveling-carrier photodiodes (UTC-PDs) (NEL, IOD-PMJ-13001) for terahertz frequency generation with soliton crystal states. As shown in Fig. 2c, e, two identical Kerr comb-based terahertz sources (KCTSs) are built, based on Comb #1 and Comb #2, which features identical noise performance, for the operation at terahertz frequency from 283 to 384 GHz, occupying the typical terahertz communication spectra allocated by the World Radiocommunication Conferences and the IEEE 802.15.3d standard. The terahertz-interval comb lines are filtered out by using a waveshaper (WS 4000A) with a high side mode suppression ratio over 54 dB (see details in Supplementary Information) and then amplified, and converted to a terahertz wave by a UTC-PD in each KCTS. Figure 2f shows the detected power of the generated terahertz wave as a function of input optical power on UTC-PD. The maximum output power is around −10 dBm at 283 GHz and 303 GHz, and the 303 GHz signal can be further amplified by a terahertz low-noise amplifier (LNA) (RPG, H-LNA 250-350) with a maximum output power of −2.48 dBm. Although the LNA has entered the saturated operating region at this output power, a minor power loss for the terahertz tone does not affect the phase noise performance evaluation.

The noise performance of the KCTS can be measured by directly beating the terahertz waves from two sources using a terahertz balanced mixer (BAM) (VDI, WR2.8BAMULP), as shown in Fig. 3b. In this case, the phase noise of microwave intermediate frequency (IF) signal is the sum of those of two KCTSs. This approach does not involve an extra microwave source, so that the actual phase noise of KCTS can be directly derived. In addition to the direct beating measurement using two KCTSs, we also attempt to measure the phase noise of KCTS #1 using the standard harmonic mixing method based on an integrated harmonic mixer (IHM) (OML, C02.8DAS02) with 24-time multiplication, where a Rubidium-clock-referenced desk-top microwave source (R&S SMAB-B167) is used as the local oscillator (LO), as shown in Fig. 3b. The LO frequency is set to 13.5 GHz, so that the microwave IF outputs are matched around 20 GHz in both cases for a fair comparison. We confirm that the down-conversion signals in both measurements are spurious-free by measuring their spectra using ESA (see details in Supplementary Information).

The red and blue curves in Fig. 3c show the RF spectra of the down-converted microwave signals in the cases of direct beating and harmonic mixing measurements, respectively. 10 kHz resolution bandwidth is used in both measurements, and the RF spectra are plotted with peak power normalized. While the direct beating signal shows a high SNR of around 80 dB, the harmonic mixing signal has a higher noise floor over the whole span of 10 MHz in the measurement. Figure 3d shows the results of the phase noise measurements in both cases. The phase noise of the LO microwave source is scaled to a carrier frequency of its 24th harmonics as a reference, which is plotted in gray curve. The noise results at offset frequencies below 10 kHz in both measurements align well and are higher than the microwave reference, as the pump noise limits the noise performance of KCTS to reach quantum limit. While at higher offset frequency over 10 kHz, the noise for harmonic mixing in blue is higher than that of direct beating in red, and comparable with the scaled LO microwave source in gray. This result shows that our KCTSs surpass conventional microwave electronics in noise performance. Note that although the mixer integrated into the IHM receiver may be different from the BAM, this does not affect our conclusion, because the mixing noise is not the dominant role in both cases. It is also interesting to compare such noise

performance with that of the 10.1 GHz fundamental repetition rate. If we scale the terahertz carrier frequency to 10.1 GHz, the measured phase noise based on the direct beating can be recalculated as −100 dBc/Hz at 1 kHz, −125 dBc/Hz at 10 kHz, −153 dBc/Hz at 100 kHz, and −162 dBc/Hz noise floor. These results agree well with the corresponding noise values for 10.1 GHz fundamental repetition rate, which are −106 dBc/Hz, −133 dBc/Hz, −141 dBc/Hz, and −160 dBc/Hz, according to Fig. 3a. This indicates that it is capable for us to generate low-noise microwave signal over a broad spectrum up to terahertz based on a single Kerr comb device, due to its universal low-noise performance over single soliton state to soliton crystal state.

The inset of Fig. 3d shows the measured Allan deviation of terahertz frequency with free-running state derived from direct beating signal, and the frequency instability is below 7×10^{-10} at 1 s and 5×10^{-9} at 100 s averaging time, respectively, indicating a high-frequency stability of our KCTS.

The low-noise and high-frequency nature of our Kerr comb source is essential for high channel data rate, and is tested by the terahertz wireless communication. Here we focus on a single wavelength and single polarization coherent communication architecture, as the wavelength and/or polarization multiplexing can always be applied once single channel performance is verified[38–40]. The experimental setup is shown in Fig. 4a. The optical transmitter is built based on KCTS #2, where an IQ modulator is introduced to load the ultra-wideband complex baseband signal on one of the two optical tones (marked in Fig. 2c). Taking advantage of the broadband optical modulation, 23 and 40 GBd baud rates are used in our experiment, which are equivalent to 8.1% and 14.1% of the transmitting carrier frequency at 283 GHz, respectively. The two tones are re-combined and transmitted over 10-km single-mode fiber (SMF), before being amplified and sent into a UTC-PD[41]. The generated 283 GHz terahertz signal is delivered over a 4-m wireless link (Fig. 4b). Terahertz antennas and lenses are deployed to collimate the terahertz beam for low-loss free-space propagation. This experiment is conducted under near-field communication conditions, which can refer to the detailed analysis in the Supplementary Information.

At the terahertz wireless receiver, KCTS #2 at 303 GHz with power amplified, serves as the LO, which is mixed with the received 283 GHz signal by using a BAM for coherent terahertz detection[42]. The down-converted IF signal with carrier frequency specifically at 20.248016 GHz is first amplified by a wideband electrical amplifier (EA) and then fed into a real-time digital storage oscilloscope (DSO) (Keysight, UXR0594A) for analog-to-digital conversion and further offline processing. The modulation baud rate is fundamentally limited by twice the IF signal carrier frequency of around 40 GBd, so that we start with 23 GBd (roll-off factor 0.1), and the spectra of captured IF signal shows a guard band of 7.6 GHz between the zero frequency and signal edge, as expected. Then we push the baud rate close to the limit with 40 GBd (roll-off factor 0.01). As shown in Fig. 4c, attributed to the high spectral stability of KCTSs, a small but clear guard band as narrow as 50 MHz is enough for signal demodulation. It helps to take full use of the spectrum and reduce the demand for the operation bandwidth of the analog-to-digital converter at the receiving end. Note that several spurious tones can be observed in Fig. 4c, mainly due to the clock leakage from the AWG and DSO. The detailed experimental configuration and DSP routine for our transceiver are described in the "Methods" section.

We plot the constellation and eye diagrams in Fig. 4d, under a 23-GBd transmission baud rate and 12-dBm launched optical power into the UTC-PD. Benefiting from the low-noise nature of our KCTSs, clear constellation and eye diagrams for three different modulation formats, including quadrature phase shift keying (QPSK), quadrature amplitude modulation (QAM) with 16-ary (16QAM) and 64-ary (64QAM) signals, are achieved. We evaluate the bit error rate (BER) versus the optical power launched into the UTC-PD for 23 and 40 GBd transmission baud
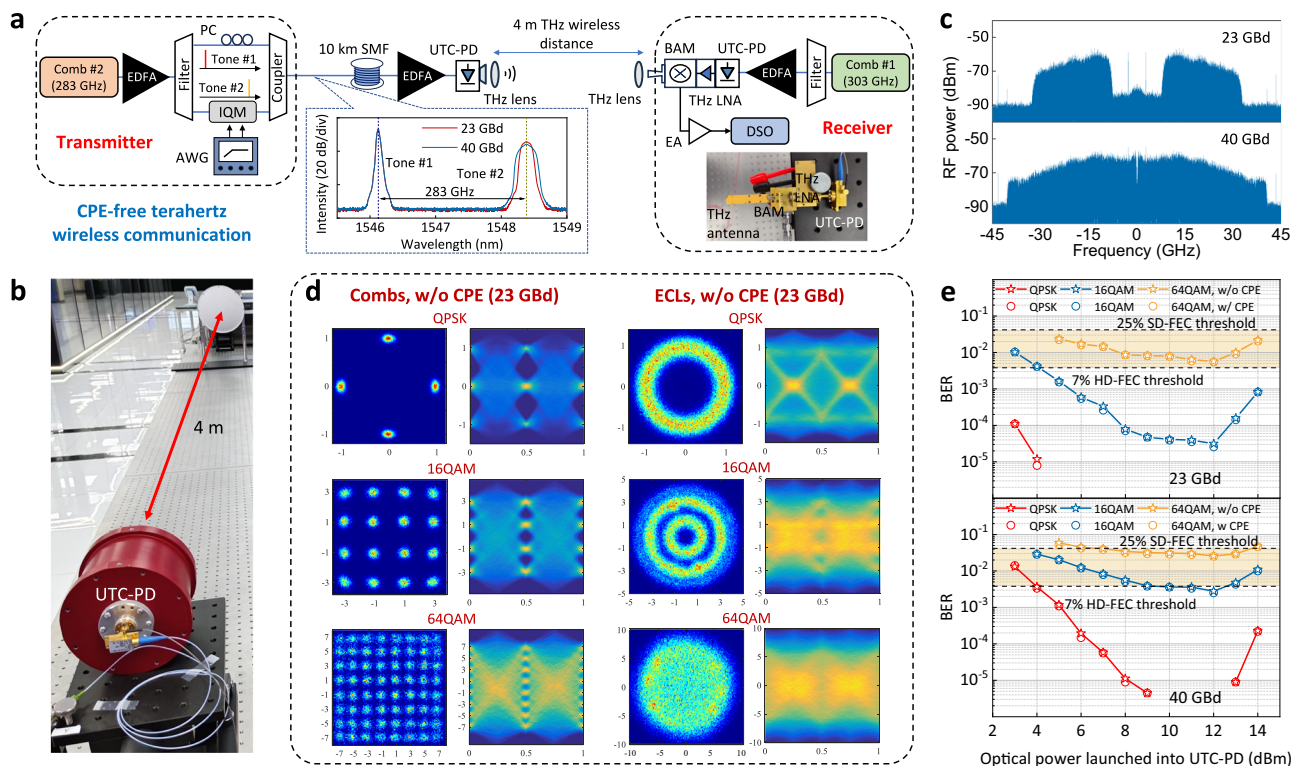
Fig. 4 | Kerr comb-driven CPE-free terahertz wireless communication.
a Experimental setup of terahertz wireless communication based on our Kerr combs. One Kerr comb with the repetition rate of 283 GHz, marked as Comb #2, is used as the coherent modulation light source to generate a 283 GHz terahertz signal at the optical transmitter. Another Kerr comb with the repetition rate of 303 GHz, marked as Comb #1, serves as the coherent light source to produce a high-purity 303 GHz terahertz LO carrier at the terahertz wireless receiver. The transmission links consist of a 10-km single-mode fiber (SMF) link and a 4-m terahertz wireless link. Inset: optical spectra of the combined two comb lines. AWG arbitrary waveform generator (Keysight, M8196), PC polarization controller, EA electrical amplifier. **b** Picture of the 4-m terahertz wireless link. **c** Down-converted IF signals captured by the real-time DSO. **d** Comparison of constellation and eye diagrams for coherent terahertz communication without CPE employing either our Kerr comb or two independent narrow-linewidth ECLs at the optical transmitter. The wireless transmission link and the terahertz wireless receiver remain unchanged from Fig. 4a. All results are measured at the same 23-GBd transmission baud rate and fixed 12-dBm launched optical power into the UTC-PD. **e** Measured BER as a function of the optical power launched into the UTC-PD, for three different modulation formats under two different baud rates. The BER performances with (w/) and without (w/o) carrier phase estimation (CPE) are both given in each case.

rates. The measured BERs of three modulation formats are shown in solid lines with stars in Fig. 4e. It is worth noting that the CPE processing is removed at the Receiver DSP for this measurement. For QPSK and 16QAM signals, both the 23- and 40-GBd cases can meet the BER threshold of 7% overhead hard-decision forward error correction (HD-FEC), i.e., 3.8×10^{-3} (lower boundary of the colored area in Fig. 4e), and the QPSK signal can even achieve error-free transmission. For 64QAM signal, both the two baud rate cases can reach 25% overhead soft-decision FEC (SD-FEC) BER threshold (i.e., 4.2×10^{-2}), upper boundary of the colored area in Fig. 4e. As a result, the line rate of the 40-GBd 64QAM signal is 240 Gbps. After subtracting 25% FEC overhead and 3% training symbols, the net rate corresponds to 186.24 Gbps. To the best of our knowledge, this is a new record of communication rate at the terahertz band driven by OFCs.

We also compare this KCTS-based terahertz communication with the normal photonics-assisted terahertz communication using dual lasers. Two independent narrow-linewidth external cavity lasers (ECLs, Realphoton TSL-PM-20) with linewidths less than 100 kHz serve as Tone #1 and Tone #2 at the optical transmitter, respectively. Under the same transmission baud rate and launched optical power into the UTC-PD, severe phase noise causes the constellation diagrams to form one or more rings (see Fig. 4d) according to the modulation format employed. This is the reason why CPE processing, including frequency offset estimation (FOE) and phase noise compensation (PNC), has to be introduced for the normal photonic-assisted terahertz communication using dual lasers. The CPE process can effectively compensate for the frequency drift and phase fluctuation, especially for the high-order modulation format case that is vulnerable to the phase noise. However, the typical CPE algorithms, such as blind-phase search, are usually power hungry, which is the main source of power consumption and cost in the receiver. Additionally, the parameter of CPE algorithms (such as sliding window length) varies with the transmitted baud rate, modulation format, and the status of link impairment, which drastically reduces the robustness and universality of the terahertz wireless receiver. For our technology using KCTSs, it is still interesting to see how much performance gain can be achieved using CPE processing. We test the BER with CPE processing for comparison, which is normally adopted in most terahertz wireless communication systems, as plotted in dashed lines with circles in Fig. 4e. The performances of these two cases (w/ and w/o CPE) are very close for all the modulation formats and baud rates. The above results again show that our KCTSs already have low enough phase noise so that normal CPE processing does not benefit over the already good BER performance. This is the fundamental advantage that the high SNR required for high-bandwidth terahertz communication can be achieved without CPE processing, besides the common advantage for the photonics-assisted terahertz communication with high modulation speed, high stability, and low power consumption, etc[43–46]. These features highlight the future terahertz terminals for both performance and low size, weight, power, and cost (SWaP-C).

Table 1 compares the key parameters of reported KCTSs with free-running operation, and our results outperform all others. Table 2

Table 1 | Comparison of KCTS performances

Kerr resonator	Quality factor (×10⁶)	Terahertz frequency (GHz)	Phase noise[a] (dBc/Hz) @ 10 kHz	Phase noise floor[a] (dBc/Hz)	Allan deviation (×10⁻¹⁰) @ 1 s	Package size of Kerr comb (mL)	Reference
FFPR	600	303	-95	-133	7	190	This work
Silica microtoroid	400	331	-72	-119	50	N/A	Opt. Express 27, 35257 (2019)
Silicon Nitride microring	1.9	300	-60	-100	200	N/A	Nat. Photonics 15, 516–522 (2021)
Silicon Nitride microring	2.2	100	-66	-106	2000	N/A	Light Sci. Appl. 10, 4 (2021)
Silicon Nitride microring	1	560	-75	-130	1000	N/A	Commun. Phys. 5, 312 (2022)
Silicon Nitride microring	N/A	300	-53	-90	N/A	N/A	APL Photonics 8, 066106 (2023)
Silicon Nitride microring	N/A	300	-50	-95	10	N/A	Opt. Lett. 45, 4377 (2020)
Silicon Nitride microring	N/A	300	-60	-90	15	N/A	arXiv:2210.15881 (2022)

[a]All the phase noise data are measured with the free-running state and scaled to a 300 GHz carrier frequency.

compares the key parameters of reported photonics-assisted terahertz wireless communications. Benefiting from the low phase noise property, our results demonstrate clear advantages in bit rate, with not only the most compact system setup, but also the simplest DSP at the Receiver.

Discussion

In conclusion, we have developed a new Kerr comb geometry using few-mode-fiber-based FFPR, following the noise modeling with limited pump power. High-Q fabrication is achieved by the state-of-the-art polishing and coating techniques to enable DFB laser diode pumping. As a result, near-quantum-limited low-noise frequency synthesis from 10.1 to 384 GHz is achieved, surpassing the noise performance of conventional microwave electronics, for the first time in a single compact electric-driven turnkey Kerr comb package. High data rate coding is achieved as a result of the combination of high carrier frequency and low phase noise performance, as demonstrated in the high-order modulated terahertz wireless communication, supporting up to 64QAM modulation and 240 Gbps data rate. Such a result is achieved without the burden of extra CPE on the DSP at the Receiver, which is required in the case of two independent narrow-linewidth lasers. Consequently, our Kerr comb not only simplifies the optical setup but also the DSP requirement, which can significantly reduce the system complexity and improve the energy efficiency. Such advantages will be even more prominent once the OFC-driven superchannel solution[47–49] is adopted in the terahertz wireless communication system. These results mark a significant step towards the practical application of the Kerr comb for high-frequency microwave applications.

Although the noise performance is already considerably low as a compact electric-driven device, it can be further improved by fabrication optimization. Our current FFPR technology is coating reflection-limited at finesse around 31,000, and a Kerr comb with a fundamental repetition rate up to 30 GHz can be realized within a 100 mW level power budget with such finesse limit. With improved polishing and coating techniques, much higher Q can be expected, within the fiber-propagation-loss Q limit on the order of 10^{11}. The improved Q will lead to the access of even lower quantum noise limits, and enable higher fundamental repetition rates for even smaller compact setup sizes. Also, higher Q helps to lower the pump power consumption and achieve higher conversion efficiency for amplifier-free operation in frequency synthesis applications. By optimizing the self-injection locking loop design and utilizing passive filters, the reduction of overall system complexity can be expected.

In this work, we mainly focus on the free-running performance of our Kerr comb, and lower noise can be achieved with active feedback control. We test the fast tuning capability of this Kerr comb by the direct modulation of drive current for the pump diode, and 10^{-7} frequency modulation can be achieved. Such a modulation range is larger than the long-term drift of our Kerr comb and forms the basis of the active feedback locking to fully stabilize this Kerr-comb-based frequency synthesizer. With these device improvements and active locking, the most demanding radar and remote sensing requirements may be fulfilled, taking advantage of such an integrated high-frequency photonics microwave source.

Methods

Detailed setup configuration for terahertz wireless communication

Our experimental setup is shown in Fig. 4a. Adding two 40 GHz phase shifters can overcome the IQ phase mismatch in the analog domain in advance during IQ modulation, which helps to improve the modulation performance of wideband signals. To achieve the best photo-mixing performance at the UTC-PD, the carrier-to-signal power ratio is set to unity, and a PC is added in Tone #1 path to align the polarization

Table 2 | Comparison of photonics-assisted terahertz wireless communications

Method	Terahertz frequency (GHz)	Phase noise floor[a] (dBc/Hz)	Bit rate (Gbps)	Measurement condition	DSP	Reference
Kerr comb (packaged)	303	−133	240	@BER 4.2 × 10⁻²	Simplified (CPE free)	This work
Kerr comb	560	−125	2	Not given BER	Not given	Opt. Continuum 2, 1267-1275 (2023)
Mode-locked laser	110	−101	40	Not given BER	Not given	Opt. Express 21, 23950-23962 (2013)
Optoelectronic oscillator-driven OFC	242	−110	24	@BER 3.8 × 10⁻³	With CPE	J. Lightw. Technol. 38, 5240–5247 (2020)
Electro-optic OFC	159	−70	0.1	@BER 1.25 × 10⁻²	Not given	IEEE Trans. Terahertz Sci. Technol. 11, 261–268 (2021)
Injection-locked DFB laser	192	−94	60 (20×3λ)	@BER 2.0 × 10⁻⁵	With CPE	IEEE Trans. Terahertz Sci. Technol. 5, 590–597 (2015)
Injection-locked dual DFB lasers	408	−112	157	@BER 2.7 × 10⁻²	With CPE	Nat. Commun. 13, 1388 (2022)
Injection-locked dual diode lasers	300	−90	80	@EVM 11.9%	Online	APL Photonics 8, 066106 (2023)
Dual Brillouin lasers	300	N/A	115	@EVM 8.7%	Online	OFC Technical Digest Series, Th1I.4 (2023)
Dual Brillouin lasers	275	−126	240	@BER 3.8 × 10⁻³	Online	IEICE Electron. Express 21, 20230584 (2023)

[a]All the phase noise data are scaled to 300 GHz carrier frequency.

between the two tones. The two identical UTC-PDs we used in this paper feature a typical responsivity of 0.22 A/W and a maximum output power of −7 dBm. To prevent the UTC-PD from being damaged, the launched optical power is controlled under 14 dBm. The generated 283 GHz terahertz signal based on the Comb #2 is then transmitted over 4-m wireless distance, corresponding to a free-space path loss of about 93.5 dB. To combat the high path loss of transmitted terahertz signal, one high gain cylindrical lens horn antenna with a gain of 48 dBi at the terahertz emitter (see Fig. 4b), and a homemade 40-dBi gain dielectric plano-convex Teflon lens with a diameter of 30 cm and a focal length of 50 cm[50], as well as a 26-dBi gain pyramidal antenna at the terahertz receiver are employed in our experiment. The above wireless configuration setup also supports terahertz long-distance delivery as long as combined with a terahertz LNA. This has already been proven by our previous work, in which the 50-Gbps terahertz signal transmission over 850 m at the 320 GHz band is successfully demonstrated[50]. At the terahertz wireless receiver, two optical tones originating from the Comb #1 are fed together into the UTC-PD with a fixed total power of 12 dBm. The generated 303 GHz terahertz carrier is boosted to −3 dBm by a terahertz LNA. Such a terahertz LO power enables the BAM to achieve the optimal electrical mixing performance. The output IF signal is then amplified by a wideband baseband EA with a gain of 35 dB before being captured by the real-time DSO.

Detailed DSP routine

At the transmitter, the ultra-wideband complex baseband signal is generated in offline MATLAB. A pseudo-random binary sequence is first mapped into the QPSK or QAM symbols. After being upsampled by two samples per symbol, all the symbols then undergo anti-aliasing processing through a root-raised-cosine (RRC) filter. Considering the bandwidth limitations of the system, different roll-off factors of the RRC filter are selected according to different baud rates. To be specific, the baud rate of 23 GBd corresponds to 0.1, while 0.01 is set for the 40-GBd case. A synchronous sequence with a length of 4096 is added prior to the information-bearing symbols, which is used for frame synchronization. After being resampled to 92 GSa/s, the data frame with a total symbol length of 2^{18} are fed into the AWG with a sample rate of 92 GSa/s and the 3-dB analogy bandwidth of 32 GHz. At the receiver, the real-time DSO with an operating bandwidth of 59 GHz and a sample rate of 128 GSa/s is used to capture the received data stream. The obtained stream is first down-converted to baseband, and then resampled to twice the symbol rate. Following frame synchronization, the Gram-Schmidt orthogonalization procedure is used to compensate for the residual IQ imbalance of the transmitted complex baseband signal, and the timing error between transceivers is overcome by the square timing recovery algorithm. Then the obtained signal is directly fed to a data-aided nonlinear equalizer after matched filtering and down-sampling. To compensate for the linear and nonlinear impairments as well as the small residual phase noise in our optical-wireless integration transmission system, while also considering the algorithm time complexity, an adaptive third-order Volterra nonlinear equalizer with the memory length of [81, 5, 3] is employed. About 3000 training symbols (accounts for 3% of the total symbols) are used to pre-converge the tap coefficients of the above equalizer, then they are adaptively updated based on the recursive least squares algorithm according to the direct-decision errors of remaining symbols. Of note, thanks to the ultra-low phase noise Kerr combs and adaptive equalizer employed in the receiving and/or transmitting ends, the conventional CPE algorithms, including FOE and PNC, can be completely dispensed with here, which significantly simplifies our receiving DSP. Finally, the BER is calculated.

Data availability

All data are available in the main text or the Supplementary Information.

References

1. Daryoosh, S. *Handbook of Terahertz Technology For Imaging, Sensing And Communications* (Woodhead Publishing, 2013).
2. Kleine-Ostmann, T. & Nagatsuma, T. A review on terahertz communications research. *J. Infrared Millim. Terahertz Waves* **32**, 143–171 (2011).
3. Seeds, A. J., Shams, H., Fice, M. J. & Renaud, C. C. Terahertz photonics for wireless communications. *J. Light. Technol.* **33**, 579–587 (2015).
4. Nagatsuma, T., Ducournau, G. & Renaud, C. C. Advances in terahertz communications accelerated by photonics. *Nat. Photonics* **10**, 371–379 (2016).
5. Akyildiz, I. F., Han, C., Hu, Z., Nie, S. & Jornet, J. M. Terahertz band communication: an old problem revisited and research directions for the next decade. *IEEE Trans. Commun.* **70**, 4250–4285 (2022).
6. Sengupta, K., Nagatsuma, T. & Mittleman, D. M. Terahertz integrated electronic and hybrid electronic–photonic systems. *Nat. Electron.* **1**, 622–635 (2018).
7. Jepsen, P. U., Cooke, D. G. & Koch, M. Terahertz spectroscopy and imaging–modern techniques and applications. *Laser Photonics Rev.* **5**, 124–166 (2011).
8. Shannon, C. E. A mathematical theory of communication. *Bell Syst. Tech. J.* **27**, 379–423 (1948).
9. Shannon, C. E. Communication in the presence of noise. *Proc. IEEE Inst. Electr. Electron. Eng.* **37**, 10–21 (1949).
10. Hartley, R. V. L. Transmission of Information 1. *Bell Syst.Tech. J.* **7**, 535–563 (1928).
11. Ye, J. & Cundiff, S. T. (eds) *Femtosecond Optical Frequency Comb: Principle, Operation and Applications* (Springer Science + Business Media, 2005).
12. Udem, T. H., R. Holzwarth, R. & Hänsch, T. W. Optical frequency metrology. *Nature* **416**, 233–237 (2002).
13. Benedick, A. J., Fujimoto, J. G. & Kärtner, F. X. Optical flywheels with attosecond jitter. *Nat. Photonics* **6**, 97–100 (2012).
14. Liang, W. et al. High spectral purity Kerr frequency comb radio frequency photonic oscillator. *Nat. Commun.* **6**, 7957 (2015).
15. Xie, X. et al. Photonic microwave signals with zeptosecond-level absolute timing noise. *Nat. Photonics* **11**, 44–47 (2017).
16. Diddams, S. A., Vahala, K. & Udem, T. Optical frequency combs: coherently uniting the electromagnetic spectrum. *Science* **369**, eaay3676 (2020).
17. Liu, J. et al. Photonic microwave generation in the X- and K-band using integrated soliton microcombs. *Nat. Photonics* **14**, 486–491 (2020).
18. Kippenberg, T. J., Gaeta, A. L., Lipson, M. & Gorodetsky, M. L. Dissipative Kerr solitons in optical microresonators. *Science* **361**, eaan8083 (2018).
19. Chang, L., Liu, S. & Bowers, J. E. Integrated optical frequency comb technologies. *Nat. Photonics* **16**, 95–108 (2022).
20. Bao, C. et al. Quantum diffusion of microcavity solitons. *Nat. Phys.* **17**, 462–466 (2021).
21. Matsko, A. B. & Maleki, L. On timing jitter of mode locked Kerr frequency combs. *Opt. Express* **21**, 28862–28876 (2013).
22. Kittlaus, E. A. et al. A low-noise photonic heterodyne synthesizer and its application to millimeter-wave radar. *Nat. Commun.* **12**, 4397 (2021).
23. Kuse, N. & Fermann, M. E. Frequency-modulated comb LIDAR. *APL Photonics* **4**, 106105 (2019).
24. Lima, E. S. et al. Integrated optical frequency comb for 5G NR Xhauls. *Sci. Rep.* **12**, 16421 (2022).
25. Yi, X., Yang, Q.-F., Yang, K. Y., Suh, M.-G. & Vahala, K. Soliton frequency comb at microwave rates in a high-Q silica microresonator. *Optica* **2**, 1078–1085 (2015).
26. Kippenberg, T. J., Spillane, S. M. & Vahala, K. J. Kerr-nonlinearity optical parametric oscillation in an ultrahigh-Q toroid microcavity. *Phys. Rev. Lett.* **93**, 083904 (2004).
27. Li, J., Lee, H., Chen, T. & Vahala, K. J. Low-pump-power, low-phase noise, and microwave to millimeter-wave repetition rate operation in microcombs. *Phys. Rev. Lett.* **109**, 233901 (2012).
28. Fortier, T. et al. Generation of ultrastable microwaves via optical frequency division. *Nat. Photonics* **5**, 425–429 (2011).
29. Liang, W. et al. Ultralow noise miniature external cavity semiconductor laser. *Nat. Commun.* **6**, 7371 (2015).
30. Hao, L. et al. Narrow-linewidth self-injection locked diode laser with a high-Q fiber Fabry–Perot resonator. *Opt. Lett.* **46**, 1397–1400 (2021).
31. Voloshin, A. S. et al. Dynamics of soliton self-injection locking in optical microresonators. *Nat. Commun.* **12**, 235 (2021).
32. Rempe, G., Thompson, R. J., Kimble, H. J. & Lalezari, R. Measurement of ultralow losses in an optical interferometer. *Opt. Lett.* **17**, 363–365 (1992).
33. Laurent, P., Clairon, A. & Breant, C. Frequency noise analysis of optically self-locked diode lasers. *IEEE J. Quantum Electron.* **25**, 1131–1142 (1989).
34. Camatel, S. & Ferrero, V. Narrow linewidth CW laser phase noise characterization methods for coherent transmission system applications. *J. Light. Technol.* **26**, 3048–3055 (2008).
35. Xiang, C. et al. Laser soliton microcombs heterogeneously integrated on silicon. *Science* **373**, 99–103 (2021).
36. Shen, B. et al. Integrated turnkey soliton microcombs. *Nature* **582**, 365–369 (2020).
37. Jin, W. et al. Hertz-linewidth semiconductor lasers using CMOS-ready ultra-high-Q microresonators. *Nat. Photonics* **15**, 346–353 (2021).
38. Zhu, M. et al. Ultra-wideband fiber-THz-fiber seamless integration communication system toward 6G: architecture, key techniques, and testbed implementation. *Sci. China Inf. Sci.* **66**, 110301 (2023).
39. Ding, J. et al. THz-over-fiber transmission with a net rate of 5.12 Tbps in an 80 channel WDM system. *Opt. Lett.* **47**, 3103–3106 (2022).
40. Cai, Y. et al. Real-time 100-GbE fiber-wireless seamless integration system using an electromagnetic dual-polarized single-input single-output wireless link at W band. *Opt. Lett.* **48**, 928–931 (2023).
41. Jia, S. et al. Integrated dual-laser photonic chip for high-purity carrier generation enabling ultrafast terahertz wireless communications. *Nat. Commun.* **13**, 1388 (2022).
42. Heffernan, B. M. et al. 60 Gbps real-time wireless communications at 300 GHz carrier using a Kerr microcomb-based source. *APL Photonics* **8**, 066106 (2023).
43. Heffernan, B., Greenberg, J., Hori, T., Tanigawa, T. & Rolland, A. Brillouin laser-driven terahertz oscillator up to 3 THz with femtosecond-level timing jitter. *Nat. Photonics* **18**, 1263–1268 (2024).
44. Kuse, N. et al. Low phase noise THz generation from a fiber-referenced Kerr microresonator soliton comb. *Commun. Phys.* **5**, 312 (2022).
45. Shin, D., Kim, B., Jang, H., Kim, Y. & Kim, S. Photonic comb-rooted synthesis of ultra-stable terahertz frequencies. *Nat. Commun.* **14**, 790 (2023).
46. Tetsumoto, T. et al. Optically referenced 300 GHz millimetre-wave oscillator. *Nat. Photonics* **15**, 516–522 (2021).
47. Lundberg, L. et al. Phase-coherent lightwave communications with frequency combs. *Nat. Commun.* **11**, 201 (2020).
48. Geng, Y. et al. Coherent optical communications using coherence-cloned Kerr soliton microcombs. *Nat. Commun.* **13**, 1070 (2022).
49. Torres-Company, V. & Weiner, A. M. Optical frequency comb technology for ultra-broadband radio-frequency photonics. *Laser Photonics Rev.* **8**, 368–393 (2013).
50. Li, W. et al. Photonic terahertz wireless communication: towards the goal of high-speed kilometer-level transmission. *J. Light. Technol.* **42**, 1159–1172 (2024).

Author contributions

K.J., Y.C., W.L., M.Z. and Z.X. conceived the original idea and designed the experiment. K.J., X.W., W.L. and Y.L. prepared the FFPRs sample, designed and packaged the Kerr comb engine, including the DFB laser and FFPRs. K.J., Y.C., X.Y., C.Q. and Z.Z. performed the measurement and simulation, and conducted the data analysis. K.J., Y.C., W.L., M.Z. and Z.X. wrote the manuscript. S.C., X.J., C.S., J.Y., H.L. and B.J. provided valuable feedback and comments. Z.X., M.Z., Y.H., X.Y. and S.Z. supervised the whole work. All authors contributed to the manuscript preparation.

Competing interests

The authors declare no competing interests.

Additional information

Supplementary information The online version contains supplementary material available at https://doi.org/10.1038/s41467-025-60630-7.

Correspondence and requests for materials should be addressed to Kunpeng Jia, Yongming Huang, Wei Liang, Min Zhu or Zhenda Xie.

Peer review information *Nature Communications* thanks Jijun He and the other anonymous reviewer(s) for their contribution to the peer review of this work. A peer review file is available.

Reprints and permissions information is available at http://www.nature.com/reprints

Publisher's note Springer Nature remains neutral with regard to jurisdictional claims in published maps and institutional affiliations.